Int. J. Electrochem. Sci., 13 **(2018)** 11906 – 11922, doi: 10.20964/2018.12.80

International Journal of
ELECTROCHEMICAL
SCIENCE
www.electrochemsci.org

Simultaneous Determination of Bisphenol A and Bisphenol S Using Multi-Walled Carbon Nanotubes Modified Electrode

Xue Wang[1,*], *Mengjia Li*[1], *Min Wu*[1], *Yaru Shi*[1], *Jiajia Yang*[2], *Jiajia Shan*[1], *Lifen Liu*[1]

[1] School of Food and Environment, Dalian University of Technology, Panjin 124221, China
[2] College of Materials Science and Engineering, Hebei University of Engineering, 199 South Guangming Street, Handan 056038, China
[*]E-mail: wangxue@dlut.edu.cn.

Received: 18 August 2018 / *Accepted:* 12 October 2018 / *Published:* 5 November 2018

A simple and sensitive electrochemical sensor based on multi-walled carbon nanotubes (MWCNTs) modified glassy carbon electrode was developed for the simultaneous determination of bisphenol A (BPA) and bisphenol S (BPS). The electrochemical behavior and electro-oxidation of BPA and BPS were investigated by cyclic voltammetry (CV) and differential pulse voltammetry (DPV). Experimental parameters such as pH of the buffer solution, accumulation time and scan rate have been optimized. The modified electrode exhibited outstanding electrocatalytic activity towards the oxidation of BPA and BPS and provided two separate oxidation current peaks enough to quantify BPA and BPS in mixture. The peak currents in DPV of BPA and BPS increased linearly with their concentrations in the ranges of 2×10^{-6} to 3×10^{-5} mol L^{-1} for BPA and 2×10^{-5} to 8×10^{-5} mol L^{-1} for BPS. The detection limits were 5×10^{-7} mol L^{-1} for BPA and 4×10^{-6} mol L^{-1} for BPS (S/N=3), respectively. Furthermore, the developed sensor was successfully applied in determination of BPA and BPS in river water and thermal paper samples.

Keywords: Bisphenol A; Bisphenol S; Simultaneous determination; Multi-walled carbon nanotubes

1. INTRODUCTION

Bisphenol A (2,2-bis(4-hydroxyphenyl) propane, BPA) is a kind of well-known endocrine disrupting compounds, and it has been widely used in the production of polycarbonate plastics and epoxy resins as an organic monomer for several decades [1]. These materials are extensively used in food containers, packing materials, water bottles, beverage cans, dental sealants, thermal paper, baby bottles and so on [2,3]. Resulting from the widespread use of BPA in daily products, a mass of BPA leaching from various products exist in food, environmental medium and living organisms [4-6]. Except for typical endocrine disrupting effects, BPA is suspected to be related to many diseases such as diabetes, reproductive disorders, obesity, birth defects, cardiovascular diseases and breast cancer

[7]. Because of human health and ecotoxicology risk, numbers of countries have forbidden the use of various products with BPA addition. In recent years, bisphenol S (4, 4′-sulfonyldiphenol, BPS) as a major BPA alternative, has been applied in industrialized production and daily applications [8]. Although BPS has high thermal stability, reduced biodegradability and low toxicity compared with BPA, plenty of researches show that BPS retains similar estrogenic activity, causes chronic diseases and shows environmental persistence [9,10]. Thus, until now, there is the potential risk of BPS as BPA alternative. BPA and BPS have similar chemical structure which both contain two hydroxyphenyl groups, and are called as bisphenol analogues. Bisphenol analogues, including BPA and BPS, can usually co-exist in the same environmental medium and interfere mutually in determination process due to their similar structures and properties [11]. It is necessary to develop a sensitive, accurate, and rapid analytical method for the detection of BPA and BPS.

Up to now, the methods for the determination of bisphenols, including BPA and BPS, are mainly based on chromatography and mass spectrometry, such as liquid chromatography-tandem mass spectrometry [12] and gas chromatography-tandem mass spectrometry [13]. Despite the fact that these conventional analytical techniques have advantages of high accuracy and sensitivity, they also require complex pretreatment process, time-consuming analysis, expensive instruments, special organic solvent and trained operators. Hence, electrochemical methods are used as a convenient way for the rapid detection of bisphenols.

In recent years, electrochemical sensor has shown promising potential for its advantages of simple operation, time-saving, high sensitivity and portability [14]. BPA and BPS have two phenolic hydroxyl groups, and at a certain potential the phenolic hydroxyl groups can be oxidized to quinone. BPA and BPS with good electrochemical activity can display two separated oxidation peaks by voltammetric method [15]. In order to further improve the sensitivity of electrochemical sensor, excellent electrode modified materials have drawn many attempts. CNTs offer unique properties including good electronic performance, larger specific surface area, chemical stability and rapid electrode kinetics. Therefore, CNT-based electrochemical sensors generally have high sensitivity, fast response and low detection limit [16,17].

In the present work, an electrochemical sensor based on multi-walled carbon nanotubes (MWCNTs) has been developed for simultaneous determination of BPA and BPS. The electrochemical behavior and electro-oxidation of BPA and BPS were investigated by cyclic and differential pulse voltammetry. The MWCNTs modified electrode showed enhanced electrocatalytic activity toward the oxidation of BPA and BPS. The proposed sensor showed good analytical performances with wide linear ranges, low detection limits, and had nice reproducibility and selectivity for the simultaneous determination of BPA and BPS. The proposed electrochemical sensor was successfully applied in real samples.

2. EXPERIMENTAL

2.1 Reagents and materials

BPA (99%) and BPS (99%) were purchased from J&K Scientific Ltd. (China). MWCNTs (purity>98 wt%, OD=30-50 nm, length=10-20 μm) and -COOH functionalized MWCNTs (purity>98

wt%, OD=30-50 nm, length<10 μm, -OH Content: 0.73 wt%) were purchased from Chengdu Organic Chemicals Co. Ltd (China). N, N-dimethyl formamide (DMF) was purchased from Xilong Chemical Co. China. Anhydrous methanol was purchased from Tianjing Damao Chemical Reagent Factory, Tianjing, China. 0.1 M phosphate buffer solution (PBS) was prepared from NaH_2PO_4 and Na_2HPO_4 (Sinopharm Chemical Reagent Co., Ltd., China) with Milli-Q water. All chemicals were of analytical grade and used as received. The HCl solution or NaOH solution was utilized to adjust the pH of PBS. The water used in all the experiments was Milli-Q water (>18.2 MΩ).

2.2 Apparatus and instruments

All electrochemical measurements were performed on a CHI660E electrochemical station (Shanghai Chenhua Co., China) with a conventional three-electrode system, a glassy carbon electrode (GCE, 3 mm in diameter), an Ag/AgCl (3 M KCl) and platinum wire as a working electrode, a reference electrode and a counter electrode, respectively. The morphology of carbon nanotubes was investigated by using a field-emission transmission electron microscopy (FE-TEM, FEI Tecnai G^2 F30, USA).

2.3 Fabrication of MWCNTs modified electrode

A bare GCE was first mechanically polished with alumina slurries (particle size 0.3 and 0.05 μm) until a mirror-like surface was obtained, and then the polished GCE was sonicated in water and ethanol for 2 minutes to remove the residual alumina particles from the electrode surface. The polished GCE was dried with high purity nitrogen gas. After that 2 mg of MWCNTs was added to 2 mL of DMF and ultra-sonicated for 2 hours to obtain the homogeneous suspension of MWCNTs. The polished GCE surface was coated with 8 μL of the above suspension and dried under an infrared lamp in air. This modified electrode was denoted as MWCNTs modified GCE (MWCNTs/GCE).

2.4 Preparation of real samples

Thermal papers and river water samples were used to demonstrate the applicability of the developed sensor. The collected water samples (from Lingshui River, Panjin, China) were filtered through a 0.45 μm filter to remove impurities to obtain a clear water sample. The thermal-sensitive papers were obtained from a local supermarket, Panjin, China. The receipt samples were prepared according to a previously published method with minor modification [18]. Briefly, the thermal papers were uniformly cut into small pieces (1 × 1 cm) and put into the glass vials. Every vial was filled with 5 mL of methanol as extracting solution. The mixtures were sonicated for about 1 hour and then incubated for 12 hours in a refrigerator at about +4 ℃. The extracting solution was filtered through a 0.45 μm filter to obtain a thermal paper sample.

2.5 Electrochemical measurement

CV measurements were recorded between 0 to +0.9 V for BPA and +0.2 to +1.2 V for BPS with a scan rate of 50 mV s^{-1}. DPV measurements were performed by applying a potential from 0 to +0.9 V for BPA and +0.2 to +1.2 V for BPS for at pulse amplitude of 50 mV and pulse width of 0.04 s. For simultaneous determination of BPA and BPS as a mixture, the potential range of DPV was 0 to +1.2 V. Electrochemical impedance spectroscopy (EIS) measurements were carried out in a mixture of 1 mM $[Fe(CN)_6]^{3-/4-}$ (1:1) and 0.1 M KCl solutions. The EIS was taken within a frequency range from 1 Hz to 100 kHz with applied amplitude of 5 mV.

3. RESULTS AND DISCUSSION

3.1 Characterization of MWCNTs

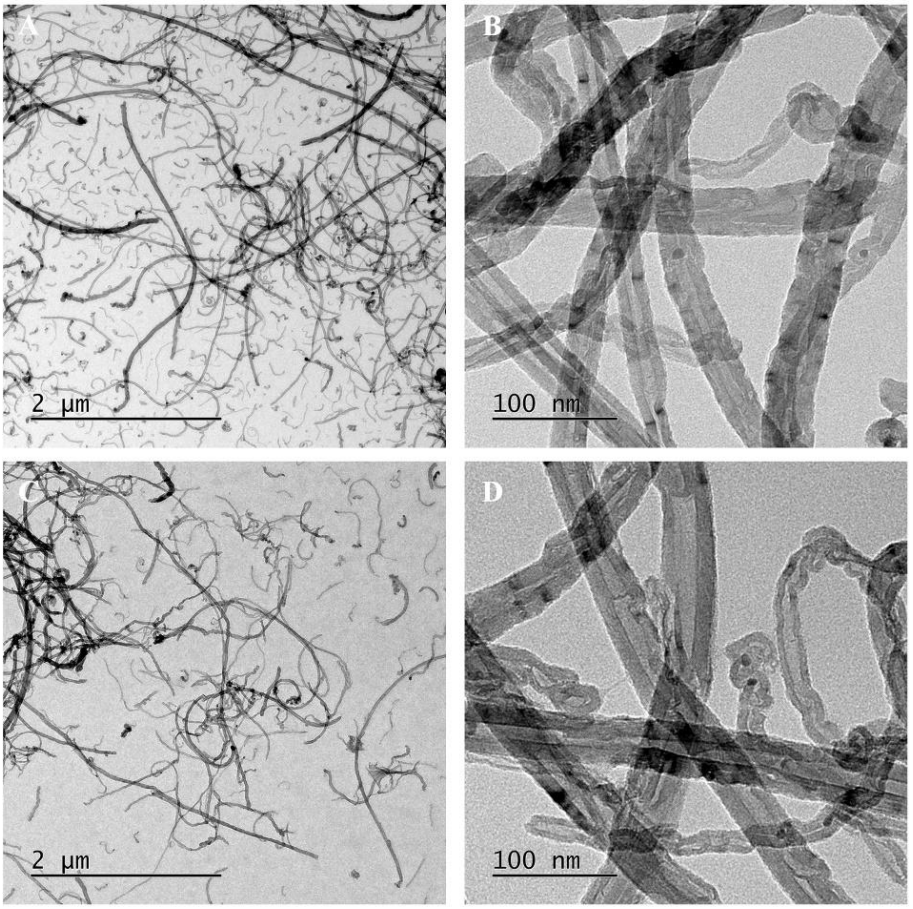

Figure 1. Different magnification TEM images of carbon nanotubes: a,b) low- and high-magnification TEM images of MWCNTs; c,d) low- and high-magnification TEM images of MWCNTs-COOH.

The MWCNTs and -COOH functionalized MWCNTs were characterized by TEM. The TEM images (Figure1) confirmed that the diameter of the MWCNTs is in the range of 30-50 nm and the

length is in the range of 10-20 μm. The diameter of the MWCNTs-COOH is in the range of 30-50 nm and the length is less than 10 μm.

3.2 Electrochemical characterization of the modified electrode

The electrochemical properties of bare electrode and modified electrodes were characterized by CV and EIS in 1 mM $[Fe(CN)_6]^{3-/4-}$ (1:1) containing 0.1 M KCl solution on bare GCE (a), MWCNTs/GCE (b) and MWCNTs-COOH/GCE (c) at a scan rate of 100 mV s^{-1}. As shown in Figure 2A, the obvious reversible one-electron redox behavior of $[Fe(CN)_6]^{3-/4-}$ is observed on the bare GCE. After being modified MWCNTs and MWCNTs-COOH, the redox peak of $[Fe(CN)_6]^{3-/4-}$ obviously increased indicating a more rapid electron transfer the modified electrodes. This phenomenon may be attributed to the excellent electrocatalytic activity, high conductivity and large specific surface area of MWCNTs and MWCNTs-COOH. Compared with MWCNTs-COOH, a lager redox peak was shown on the MWCNTs modified electrode. This result was attributed to the introduction of carboxyl and oxygen-containing groups of MWCNTs-COOH, which had an impact on the electron transfer.

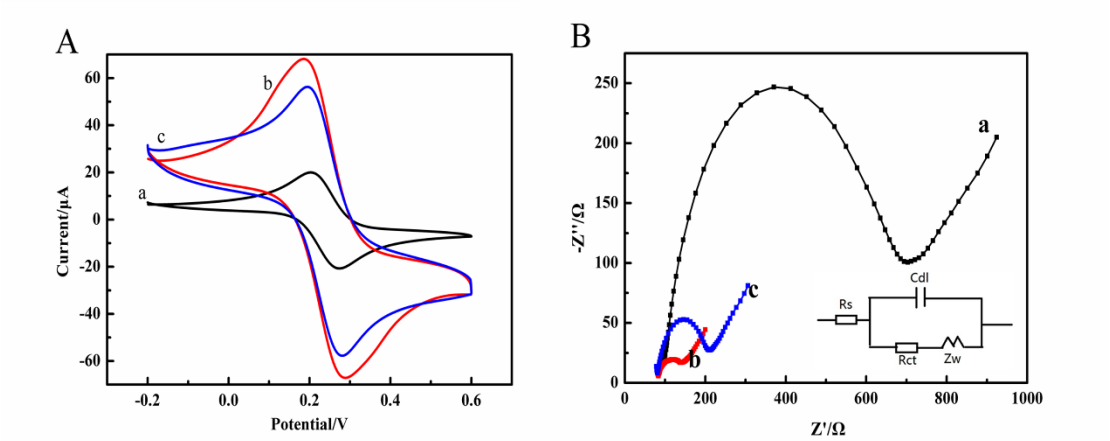

Figure 2. Cyclic voltammograms (A) and Nyquist plots (B) of different electrodes in 1 mM $[Fe(CN)_6]^{3-/4-}$ solution containing 0.1 M KCl. Scan rate: 100 mV s^{-1}. The frequency range is from 1 to 10^5 Hz with applied amplitude of 5 mV. (a) Bare GCE, (b) MWCNTs/GCE, (c) MWCNTs-COOH/GCE. Inset is the Randles equivalent circuit: R_S, electrolyte solution resistance; R_{ct}, charge transfer resistance; Z_W, Warburg impedance resulting from the diffusion of ions; C_{dl}, double layer capacitance of the electrode.

Figure 2B displays the Nyquist plots of different electrodes. By fitting the data, an equivalent circuit was established as shown in the inset of Figure 2B. The Nyquist plot of the EIS in this work includes a semicircular portion and a linear portion. The semicircle portion at higher frequencies generally indicates the charge transfer resistance (R_{ct}), and the linear portion at lower frequencies generally corresponds to the diffusion process [19]. The R_{ct} depends on the dielectric and insulating features at the electrode/electrolyte interface [20]. The largest R_{ct} was observed on the bare GCE (a), which was calculated to be 590 Ω. When MWCNTs and MWCNTs-COOH were modified on the surface of bare electrode, R_{ct} values have decreased dramatically to 80.16 Ω and 130.87 Ω,

respectively, proving a more rapid electron transfer rate. The modified materials enhanced the conductivity of electrode effectively and facilitated the electron transfer between the electrode and the redox probe.

3.3 Electrochemical behavior of BPA and BPS

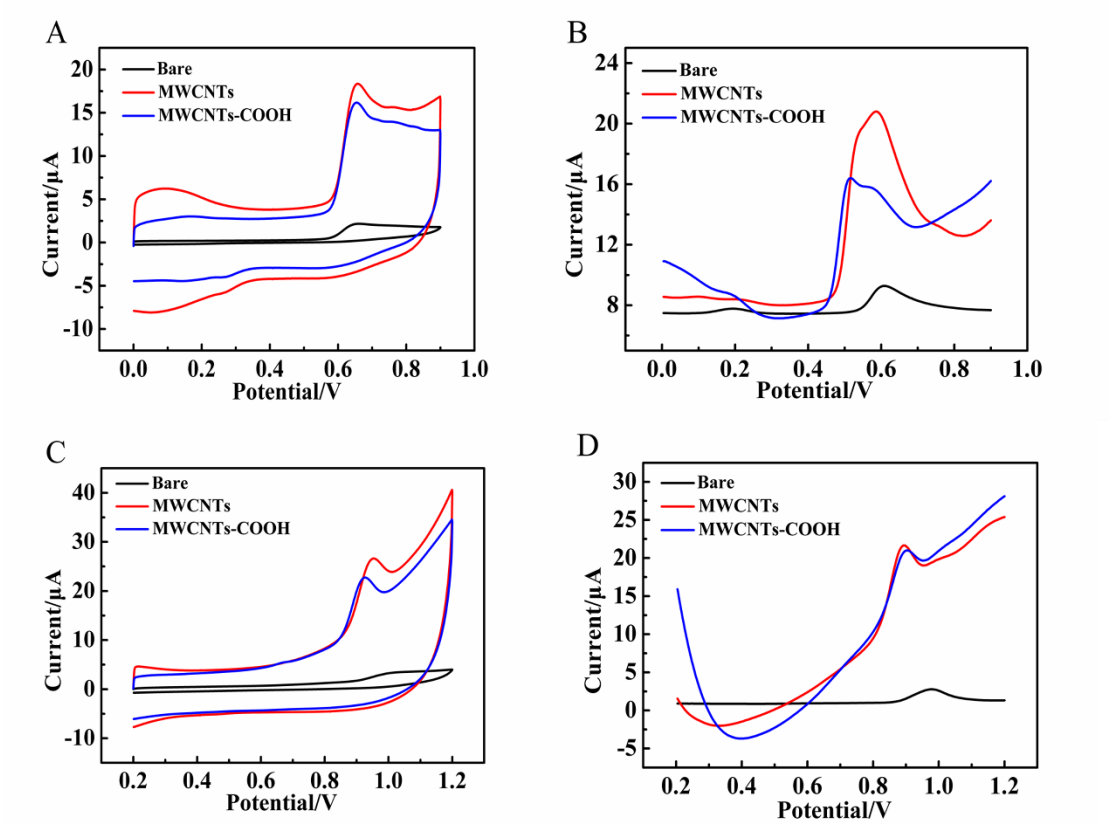

Figure 3. CV curves of 5×10^{-5} mol/L BPA (A) and BPS (C) and DPV curves of 5×10^{-5} mol/L BPA (B) and BPS (D) in 0.1M PBS (pH = 6) at bare GCE, MWCNTs/GCE and MWCNTs-COOH/GCE.

The electrochemical behavior and oxidation of BPA and BPS were assessed by CV and DPV in 0.1 M PBS (pH = 6). Figure 3A and C shows the CVs of 5×10^{-5} mol L^{-1} BPA and BPS at the bare GCE, MWCNTs/GCE and MWCNTs-COOH/GCE, respectively. It was noted that a single oxidation peak respectively appeared for BPA in the potential window from 0 to +0.9 V and BPS in the potential window from +0.2 to +1.2 V on all electrodes tested, and no reduction peak was observed in the reverse scan. The CV curves demonstrated that the electrochemical oxidation of BPA and BPS on the electrode surface was an irreversible process [21].

At bare GCE, BPA exhibited a broad anodic peak and a relatively poor electrochemical response at approximatively 0.65 V in CV curve, which indicated that the electron transfer of BPA on bare GCE was very slow. For the modified electrodes, the oxidation peak of BPA was a significant increase compared with the bare one. It was pointed out that the MWCNTs/GCE exhibited the best

performance for the oxidation of BPA with the highest peak current. For BPS, MWCNTs/GCE still exhibited the superior electrocatalytic activity with a higher electrooxidation current. In addition, regarding the peak potentials, for the modified electrodes the oxidation peak shifted negatively compared to the bare electrode, which favored the oxidation reaction. Figure 3B and D shows the DPV curves of 5 × 10^{-5} mol L^{-1} BPA and BPS at the bare GCE, MWCNTs/GCE and MWCNTs-COOH/GCE, respectively, and the result was in agreement with that obtained from CVs.

3.4 Electrocatalytic oxidation of BPA and BPS as a mixture

The response of 5×10^{-5} mol L^{-1} BPA and BPS as a mixture in PBS (pH = 6) on different electrodes was investigated by CV (Figure 4A). CVs were recorded in the potential range of 0.0 to +1.2 V. Figure 4A shows the comparison of electrocatalytic oxidation towards BPA and BPS at the bare electrode, MWCNTs/GCE and MWCNTs-COOH/GCE. Depending on Figure 4A, weak and broad peaks were observed at the bare GCE. At modified electrodes, two separated oxidation peaks were clearly observed at approximatively +0.66 V and +0.98 V (versus 3 M Ag/AgCl electrode), respectively. Compared with MWCNTs-COOH/GCE, MWCNTs/GCE provided higher peak currents, which was similar to the above individual determination.

DPV is an electrochemical analytical technique with high sensitivity and low detection limit, which has been often applied for the determination of many substances. To observe the enhanced effect of MWCNTs for electro-catalysis, DPV was carried out to study the simultaneous electrochemical determination of 5×10^{-5} mol L^{-1} BPA and BPS as a mixture on different electrodes in pH 6 PBS. As shown in Figure 4B, the DPV curve exhibited two weak anodic peaks for BPA and BPS on the bare GCE, indicating poor oxidation activity, which was disadvantageous to the sensitive detection. When applying the MWCNTs-COOH/GCE, not only the anodic peaks currents of BPA and BPS were dramatically enhanced, but also the peak potentials shifted negatively. After coating with MWCNTs, the peaks currents were further enhanced. The difference of the oxidation peak potentials of BPA and BPS was 0.32 V, which was large enough to simultaneously detect BPA and BPS.

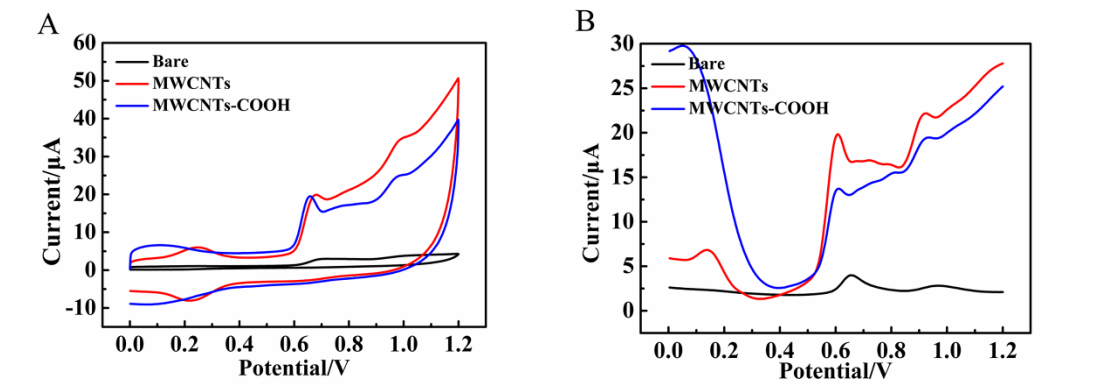

Figure 4. (A) CV and (B) DPV curves of 5 × 10^{-5} mol L^{-1} BPA and BPS as a mixture in 0.1 M PBS (pH = 6) at bare GCE, MWCNTs/GCE and MWCNTs-COOH/GCE.

3.5 Effective surface area of modified electrode

The chronocoulometry method was used to calculate the effective surface areas (A) of different electrodes in 1 mM $[Fe(CN)_6]^{3-/4-}$ (1:1) solution containing 0.1 M KCl (Figure 5A). The calculation equation was given by following Anson equation [22]:

$$Q(t) = \frac{2nFAcD^{1/2}t^{1/2}}{\pi^{1/2}} + Q_{dl} + Q_{ads}$$

Where A is the effective surface area of the working electrode, n is the number of electrons transferred, c is the concentration of substrate, D is the standard diffusion coefficient of $[Fe(CN)_6]^{3-}$ (7.6×10^{-6} cm^2 s^{-1} at 25 °C) , Q_{dl} is double layer charge, Q_{ads} is the Faradic charge. As shown in Figure 5B, the charge (Q) was linear to the square root of time ($t^{1/2}$). The linear equations were Q_{Bare} (μC) = $37.948t^{1/2}$ + 0.614 (R^2=0.9971) for bare GCE and Q_{MWCNTs} (μC) = $107.160t^{1/2}$ + 5.373 (R^2=0.9996) for MWCNTs/GCE. According to the slopes of the calibration plots, the active area for bare GCE and MWCNTs/GCE were calculated as 0.063 cm^2 and 0.179 cm^2, respectively. The active area of MWCNTs/GCE was almost 3 times greater than that of bare GCE and it was beneficial to provide more binding sites for enhancing the electrocatalytic activity of the modified electrode.

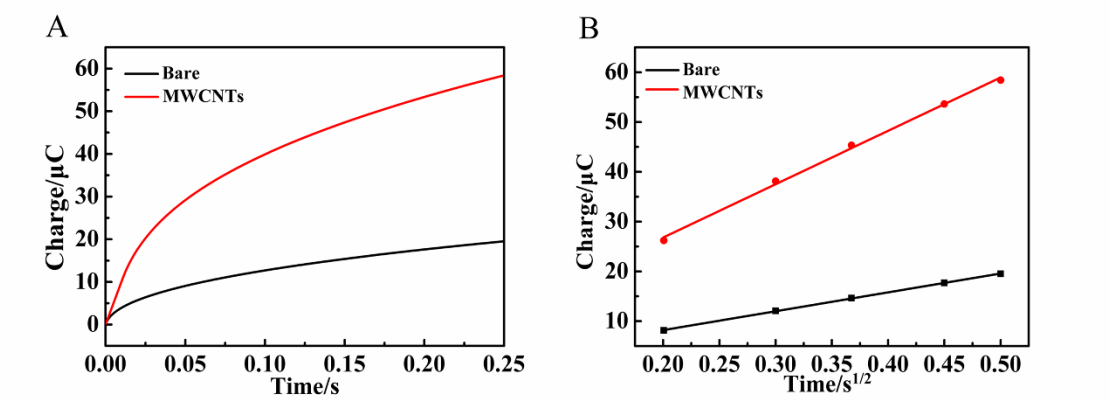

Figure 5. (A) Chronocoulometric curves of bare GCE and MWCNTs/GCE. (B) Linear relationship of *Q* and $t^{1/2}$on bare GCE and MWCNTs/GCE.

3.6 Effect of scan rate

To understand oxidation mechanism and kinetic property, CVs of MWCNT/GCE as a working electrode in PBS solution (pH = 6.0) containing 5×10^{-5} mol L^{-1} BPA and BPS with scan rates (*v*) varying from 10 to 110 mV s^{-1} were presented in Figure 6. The oxidation peak currents of BPA (Figure 6A) and BPS (Figure 6D) gradually increased with the increasing scan rate. As revealed in Figure 6B and Figure 6E, peak currents linearly increase with the increase of the scan rates, and they were described by the following equations: I_{pBPA} (μA) = 0.585 ν + 0.543 (R^2=0.9756) for BPA and I_{pBPS} (μA) = 0.308 ν + 5.736 (R^2=0.9803) for BPS, respectively. This linear relationship indicates that the electrochemical oxidation of BPA and BPS at the MWCNTs/GCE is a typical adsorption-controlled process [23,24]. Meanwhile, by increasing the scan rates, the oxidation peak potentials of BPA (E_{pBPA}) and BPS (E_{pBPS}) gradually shift to positive values. The E_{pBPA} and E_{pBPS} exhibited a linear

relationship with the logarithm of scan rates in the range of 10-110 mV s^{-1} (Figure 6C and Figure 6F). The regression equations can be depicted E_{pBPA} (V) = 0.035 lnν (mV s^{-1}) + 0.521 (R^2=0.9861) for BPA and E_{pBPS} (V) = 0.016 lnν (mV s^{-1}) + 0.792 (R^2=0.9972) for BPS. For an irreversible electrode process, the relationship between E_p and lnν can be described by Laviron equation [25]:

$$E_p = E^0 + \left(\frac{RT}{\alpha nF}\right)\ln\left(\frac{RTk_s}{\alpha nF}\right) + \left(\frac{RT}{\alpha nF}\right)ln\nu$$

Where 'α' is the transfer coefficient, 'k_s' is the standard rate constant of the reaction in s^{-1}, 'n' is the number of electrons transferred, 'υ' is the scan rate and 'E^0' is the formal redox potential. R was the gas constant, T was the absolute temperature and F was the Faraday constant. According to the linear correlation of E_p, the slope of the line was equal to RT/αnF. In our study, αn was calculated to be 0.734 for BPA and 1.605 for BPS. Generally, α was assumed to be 0.5 in the totally irreversible electrode process [26], n was calculated to be 1.47 for BPA and 3.21 for BPS, respectively.

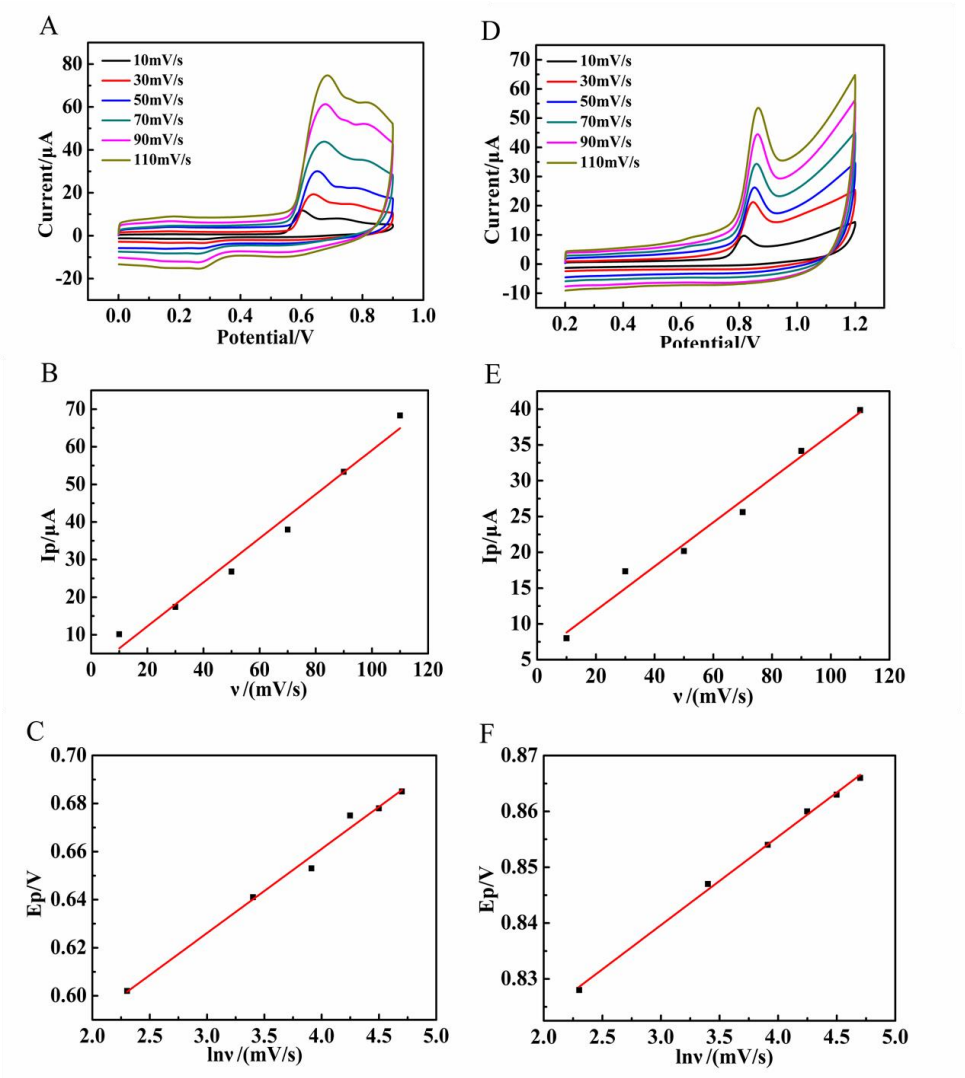

Figure 6. Cyclic voltammograms of 5×10^{-5} mol L^{-1} BPA (A) and BPS (D) at a MWCNTs/GCE with different scan rates in range of 10-110 mV s^{-1}; The relationship for BPA (B) and BPS (E) between the oxidation peak current (I) and scan rate (v); The relationship for BPA (C) and BPS (F) between the oxidation potential (E_p) and lnv.

3.7 Effect of pH

The effect of pH on the electrochemical responses of BPA and BPS at MWCNTs/GCE was studied with the pH of electrolyte solution ranging from 4.0 to 9.0 (Figure 7A and 7C). In Figure 7B, the oxidation peak currents of BPA increased gradually from pH 4.0 to pH 7.0. While the pH value was over 7.0, the peak currents reduced. In Figure 7D, the oxidation peak currents of BPS increased gradually over the pH from 4.0 to 6.0. While the pH exceeded 6.0, the peak currents decreased. The pH with maximum response was lower than the pKa of BPA (pKa = 9.73 [27]) and BPS (pKa = 8.20 [28]), indicating that the undissociated BPA and BPS could adsorb better than the dissociated chemicals on the modified electrode surface. Therefore, for the simultaneous and sensitive determination of BPA and BPS, 0.1 M PBS with the pH of 6.0 was chosen as the supporting electrolyte.

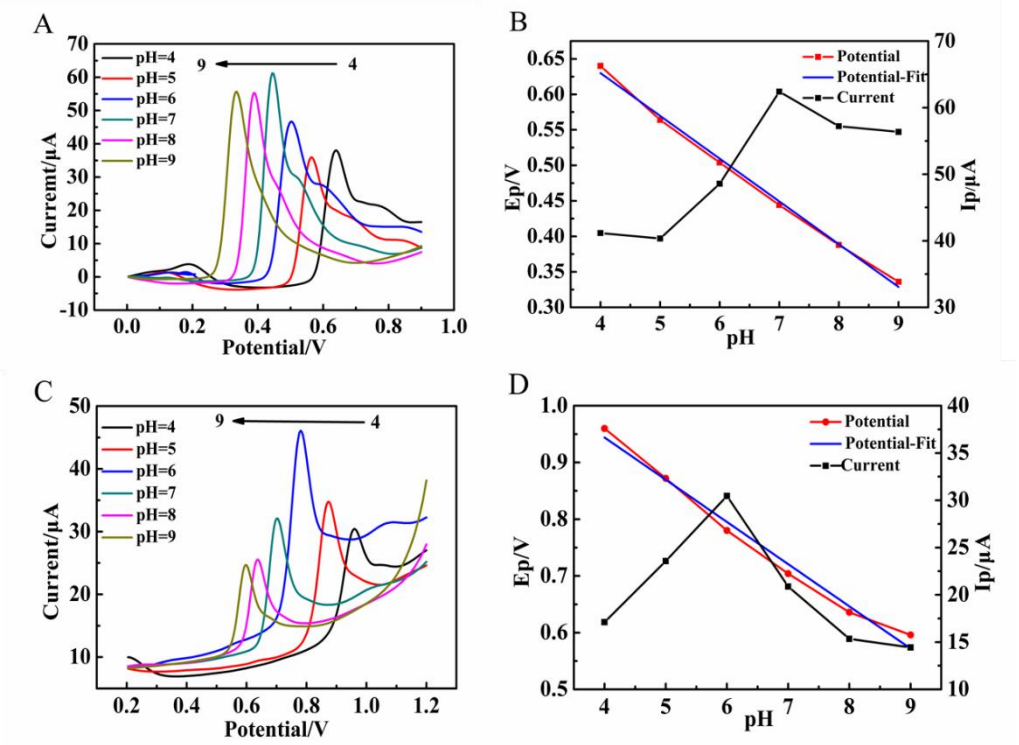

Figure 7. DPV of 5×10^{-5} mol L^{-1} BPA (A) and BPS (C) at MWCNTs/GCE in 0.1 M PBS at pH values from 4.0–9.0; Effects of pH values on the oxidation potential and peak current of 5×10^{-5} mol L^{-1} BPA (B) and BPS (D).

In addition, the relationship of peak potential vs. pH value for BPA and BPS was studied. The peak potential (E_p) shifted negatively along with the increase of pH value. A good linear relationship was obtained between the E_p and pH values (shown in Figure 7B and 7D), and the linear equations were E_{pBPA} (V) = -0.060 pH + 0.871 (R^2=0.9952) and E_{pBPS} (V) = -0.074 pH +1.242 (R^2=0.9815). The slope values of 60.0 mV pH^{-1} for BPA and 74.0 mV pH^{-1} for BPS were both approximately to the theoretical value of 57.6 mV pH^{-1}, indicating that numbers of electrons and protons were equal in the oxidation process of BPA and BPS on the modified electrode surface [29].

3.8 Effect of accumulation time

Because the electro-oxidation of BPA and BPS at MWCNTs/GCE was a typical adsorption-controlled process, the accumulation could increase the amount of BPA and BPS on the electrode surface and enhance the current response. Figure 8 illustrates the effect of accumulation time on the oxidation peak currents of BPA (Figure 8A) and BPS (Figure 8B) at MWCNTs/GCE. As shown in Figure 8A, the peak current of BPA generally increased with time and reached a plateau with an accumulation time of 120 s. With a further increase in the accumulation time, the oxidation peak current remained nearly constant. As shown in Figure 8B, the current of BPS increased gradually with accumulation time increasing from 0 to 120 s. With further increase of the accumulation time, the oxidation peak current decreased slightly. These results indicated that with the accumulation time of 120 s, the peak currents of BPA of BPS simultaneously reached the maximum value. Considering sensitivity and analysis time, 120 s was chosen as the optimal accumulation time.

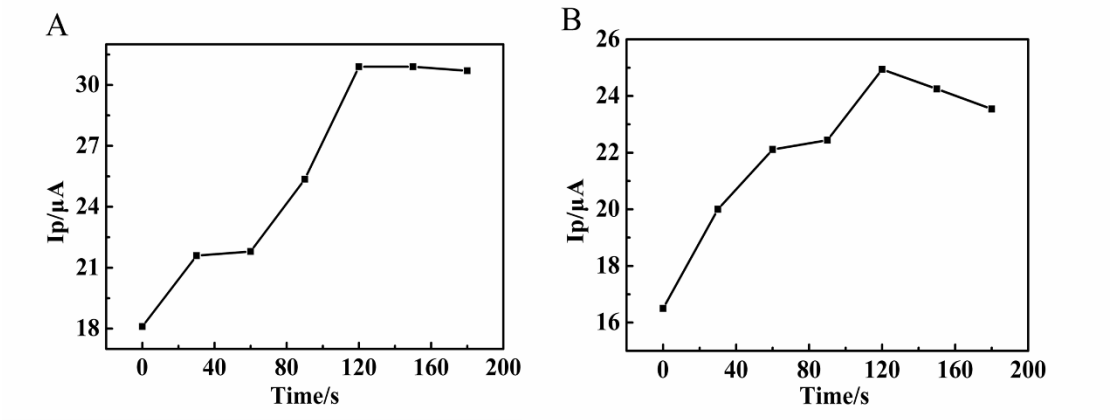

Figure 8. Effect of accumulation time on the peak currents of 5×10^{-5} mol L^{-1} BPA (A) and 5×10^{-5} mol L^{-1} BPS (B) at MWCNTs/GCE.

3.9 Simultaneous determination of BPA and BPS using MWCNTs/GCE

The simultaneous determination of BPA and BPS as a mixture was performed at the MWCNTs/GCE by DPV. The determination of BPA or BPS in their mixed solution was studied when the concentration of one species changed, the concentrations of the other were constant. Various concentrations of BPA (0 to 5×10^{-5} mol L^{-1}) were mixed with a fixed concentration of BPS (5×10^{-5} mol L^{-1}), and DPV curves are shown in Figure 9A. The DPV results show two well-separated anodic current peaks at potentials of +0.50 and +0.75 V, corresponding to the electro-oxidation of BPA and BPS, respectively. Potential difference between the two anodic peak potentials of BPA and BPS is 0.25 V that is adequate for the simultaneous determination of BPA and BPS. The oxidation peak currents of BPA showed an obvious linear relationship with the concentrations ranging from 2×10^{-6} to 3×10^{-5} mol L^{-1}, and the presence of BPS has no significant influence on the peak currents and peak potentials of BPA. The corresponding regression equation can be expressed as $i_p = 0.513c_{BPA} + 0.501$ ($R^2 = 0.9857$), and the detection limit was 5×10^{-7} mol L^{-1} (S/N=3) (Figure 9B). Similarly, various concentrations of BPS (0 to 1×10^{-4} mol L^{-1}) were mixed with a fixed concentration of BPA

(5×10^{-5} mol L^{-1}), and DPV curves are shown in Figure 9C. The oxidation peak currents of BPS showed an obvious linear relationship with the concentrations ranging from 2×10^{-5} to 8×10^{-5} mol L^{-1}. The corresponding regression equation can be expressed as $I_p = 0.188c_{BPS} - 4.188$ ($R^2 = 0.9737$), and the detection limit was 4×10^{-6} mol L^{-1} (S/N=3) (Figure 9D). The analytical performances of the prepared electrochemical sensor in this paper were compared with other similar sensors, as summarized in Table 1. Only one kind of analyte, like BPA, was noted with concern in most literature. Regarding the simultaneous detection of BPA and BPS in this paper, it can be concluded that the MWCNTs/GCE showed good analytical performances in the linear range and detection limit. In further research, composite materials based on MWCNTs can be studied for improving the performance of the electrochemical sensing platform.

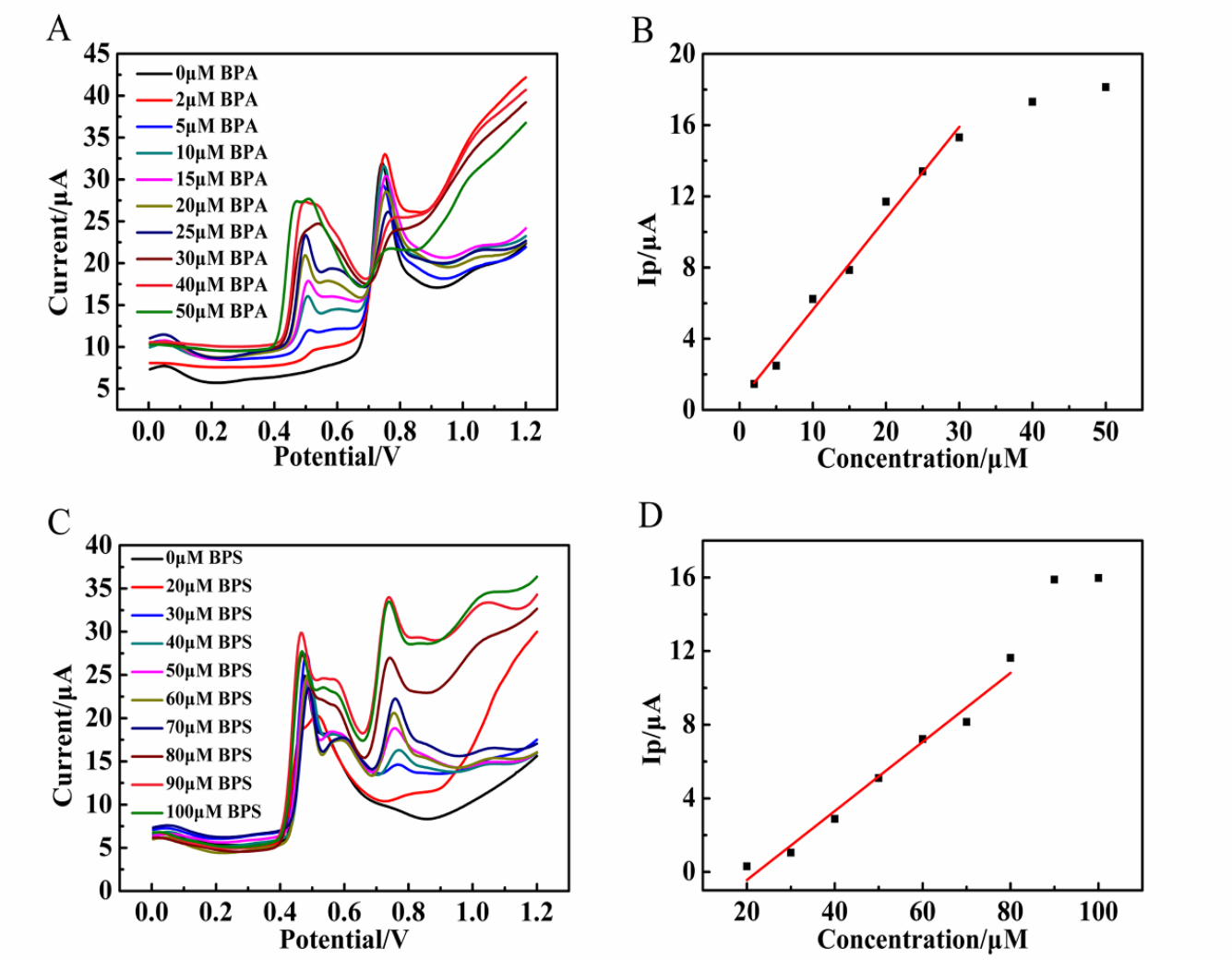

Figure 9. DPVs of BPA and BPS at different concentrations. (A) The concentrations of BPA from 0 to 5×10^{-5} mol L^{-1} in the presence of 5×10^{-5} mol L^{-1} BPS; (B) The related calibration curve of BPA; (C) The concentrations of BPS from 0 to 1×10^{-4} mol L^{-1} in the presence of 5×10^{-5} mol L^{-1} BPS; (D) The related calibration curve of BPS.

Table 1. Comparison of performances of different electrochemical sensors for determination of BPA and BPS.

Modified electrodes	Analytes	Linear range (μM)	Detection limit (μM))	Reference
Pt/PDDA-DMP/GCE[a]	BPA and BPS	5-30 for BPA, 10-60 for BPS	0.6 for BPA, 2 for BPS	[15]
SWCNT/GCE[b]	BPA	10-100	7.3	[21]
AgNP/MWCNT/GCE[c]	hydroquinone, catechol, BPA and phenol	5-152	2.4	[30]
NH_2-MIL-125/RGO/GCE[d]	BPA	2-200	0.7966	[31]
MWCNTs/GCE	BPA and BPS	2-30 for BPA, 20-80 for BPS	0.5 for BPA, 4 for BPS	This work

[a] PDDA: poly(diallyl dimethyl ammonium chloride), DMP: diamond powder;
[b] SWCNT: single-walled carbon nanotube;
[c] AgNP: silver nanoparticle;
[d] RGO: reduced graphene oxide.

3.10 Reproducibility and interference study

The reproducibility of MWCNTs/GCE was examined in the solution containing of 2.5×10^{-5} mol L^{-1} BPA and BPS (Figure 10), and the relative standard deviation (RSD) of current signals at five independently prepared modified electrode was 8.55% for BPA and 9.60% for BPS, indicating a good reproducibility.

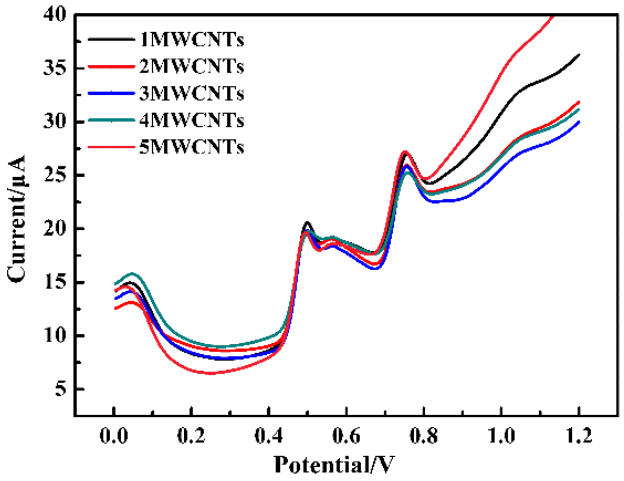

Figure 10. DPV curves of 2.5 × 10^{-5} mol L^{-1} BPA and BPS at MWCNTs/GCE in reproducibility experiments.

To evaluate specificity of the developed sensor, the influences of two typical phenolic compounds catechol (CL) and hydroquinone (HQ) were studied in this work. As shown in Figure 11, the peak potential of CL is +0.188 V, and the peak potential of HQ is +0.092 V. The result demonstrated the signals of 2.5×10^{-5} mol L^{-1} BPA and BPS were not affected by 4-fold concentration of CL and HQ. Furthermore, 100-fold concentration of SO_4^{2-}, PO_4^{3-}, NO_3^-, NH_4^+, Mg^{2+} and Ca^{2+} had little impact on the determination of BPA and BPS, indicating that MWCNTs/GCE had a good anti-interference ability.

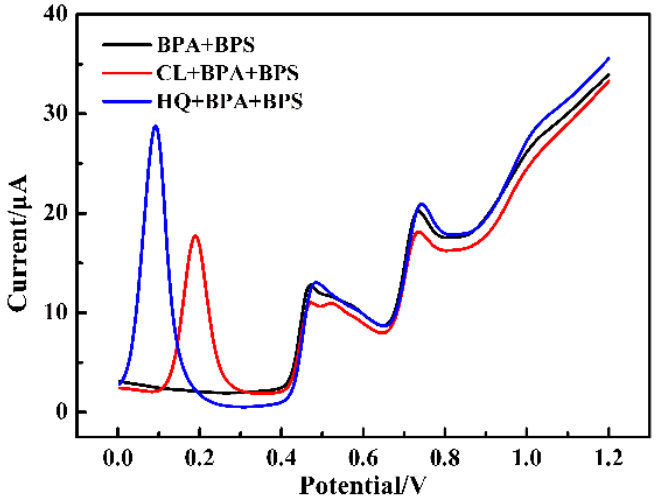

Figure 11. DPV curves of 1 × 10^{-4} mol L^{-1} CL and 1 × 10^{-4} mol L^{-1} HQ were added to a solution containing 2.5 × 10^{-5} mol L^{-1} BPA and BPS, respectively.

3.11 Analysis of real samples

To evaluate the practical application of the proposed sensor, the concentration of BPA and BPS in real samples was detected by MWCNTs/GCE. The results are shown in Table 1. BPA was detected by the MWCNTs/GCE in both river water and thermal papers after simple pretreatment, and the concentrations were 3.62 and 4.48 μM, respectively. Under the optimized conditions, a certain concentration of BPA and BPS standard solution was spiked into real samples. Recovery testing was carried out to demonstrate the validity of the proposed method. The obtained recoveries for BPA in river water were from 104.34% - 107.58% and in thermal paper samples were from 97.1% - 105.40%. The obtained recoveries for BPS in river water were from 97.30% - 106.96% and in thermal paper samples were from 102.8% - 107.35%. This result demonstrated the designed sensor had a satisfactory accuracy and recovery. Therefore, the designed sensor could meet the need for detection of BPA and BPS in real samples.

Table 2. Determination of BPA and BPS in real samples using MWCNTs/GCE.

Sample	BPA				BPS			
	Original (μM)	Added (μM)	Found (μM)	Recovery (%)	Original (μM)	Added (μM)	Found (μM)	Recovery (%)
River water	3.62	10	14.38	107.58	None	40	41.70	104.25
		15	19.75	107.52		50	53.48	106.96
		20	24.49	104.34		60	58.38	97.30
Thermal paper	4.48	10	14.19	97.10	None	40	42.94	107.35
		15	20.29	105.40		50	53.17	106.34
		20	24.86	101.90		60	61.68	102.80

4. CONCLUSIONS

In this study, MWCNTs were used to fabricate a simple and sensitive electrochemical sensor for the simultaneous determination of BPA and BPS. The electrochemical sensor based on MWCNTs shows excellent electrocatalytic activity towards the oxidation process of BPA and BPS with broad linear range and low detection limit. The proposed sensor was successfully applied for the detection of

BPA and BPS in real samples, and the acceptable recovery results proved the good practicality of this sensor.

ACKNOWLEDGEMENTS
This study is supported by National Natural Science Foundation of China (No. 21707014), the Fundamental Research Funds for the Central Universities (No. DUT18JC33), Open Foundation of Key Laboratory of Industrial Ecology and Environmental Engineering, MOE (No. KLIEEE-16-10), Natural Science Foundation of Hebei Province (No. B2017402043)

References

1. M. Thoene, L. Rytel, N. Nowicka, and J. Wojtkiewicz, *Toxicol. Res.,* 7 (2018) 371.
2. J. Zhang, X. Xu, and Z. Chen, *Ionics,* 24 (7), 2123-2134 (2018).
3. W. Zheng, Z. Xiong, H. Li, S. Yu, G. Li, L. Niu, and W. Liu, *Sens. Actuators B Chem,* 272 (2018) 655.
4. N. Salgueiro-Gonzalez, S. Castiglioni, E. Zuccato, I. Turnes-Carou, P. Lopez-Mahia, and S. Muniategui-Lorenzo, *Anal. Chim. Acta,* 1024 (2018) 39.
5. S. A. Baluka, W. K. Rumbeiha, *Food Chem. Toxicol.,* 92 (2016) 58.
6. R. Huang, Z. Liu, H. Yin, Z. Dang, P. Wu, N. Zhu, and Z. Lin, *Sci. Total Environ.,* 626 (2018) 971.
7. Y. Zhang, X. Ren, Y. Li, X. Yao, C. Li, Z. Qin, and L. Guo, *Environ. Pollut.,* 237 (2018) 1072.
8. C. Zhao, P. Xie, T. Yong, H. Wang, A. C. K. Chung, and Z. Cai, *Anal. Chem.,* 90 (2018) 3196.
9. W. Zhu, X. Yue, J. Duan, Y. Zhang, W. Zhang, S. Yu, Y. Wang, D. Zhang, and J. Wang, *Electrochim. Acta,* 188 (2016) 85.
10. H. Rao, X. Zhao, X. Liu, J. Zhong, Z. Zhang, P. Zou, Y. Jiang, X. Wang, and Y. Wang, *Biosens. Bioelectron.,* 100 (2018) 341.
11. Q. Wang, D. Zhang, L. Yang, and L. Zhang, *Sens. Actuators B Chem,* 246 (2017) 800.
12. B. A. Rocha, A. R. M. de Oliveira, and F. Barbosa, *Talanta,* 183 (2018) 94.
13. M. T. Garcia-Corcoles, M. Cipa, R. Rodriguez-Gomez, A. Rivas, F. Olea-Serrano, J. L. Vilchez, and A. Zafra-Gomez, *Talanta,* 178 (2018) 441.
14. G. Maduraiveeran, M. Sasidharan, and V. Ganesan, *Biosens. Bioelectron.,* 103 (2018) 113.
15. Z. Zheng, J. Liu, M. Wang, J. Cao, L. Li, C. Wang, and N. Feng, *J. Electrochem. Soc.,* 163 (2016) 192.
16. S. K. Vashist, D. Zheng, K. Al-Rubeaan, J. H. T. Luong, and F. S. Sheu, *Biotechnol. Adv.,* 29 (2011) 169.
17. C. B. Jacobs, M. J. Peairs, and B. J. Venton, *Anal. Chim. Acta,* 662 (2010) 105.
18. M. Lawrywianiec, J. Smajdor, B. Paczosa-Bator, and R. Piech, *Food Anal. Methods,* 10 (2017) 3825.
19. H. Bagheri, A. Hajian, M. Rezaei, and A. Shirzadmehr, *J. Hazard. Mater.,* 324 (2017) 762.
20. M. Wang, Y. Gao, J. Zhang, and J. Zhao, *Electrochim. Acta,* 155 (2015) 236.
21. P. Kanagavalli and S. S. Kumar, *Electroanal,* 30 (2018) 445.
22. N. Butwong, S. Srijaranai, J. D. Glennon, and J. H. T. Luong, *Electroanal,* 30 (2018) 962.
23. E. Asadian, S. Shahrokhian, A. I. Zad, and F. Ghorbani-Bidkorbeh, *Sens. Actuators B Chem,* 239 (2017) 617.
24. Y. Wang, C. Li, T. Wu, and X. Ye, *Carbon,* 129 (2018) 21.
25. E. Laviron, *J. Electroanal. Chem.,* 101 (1979) 19.
26. T. Zhan, Y. Song, Z. Tan, and W. Hou, *Sens. Actuators B Chem,* 238 (2017) 962.
27. Y. Li, X. Zhai, X. Liu, L. Wang, H. Liu, and H. Wang, *Talanta,* 148 (2016) 362.

28. H. Guo, H. Li, N. Liang, F. Chen, S. Liao, D. Zhang, M. Wu, and B. Pan, *Environ. Sci. Pollut. Res.*, 23 (2016) 8976.
29. H. Fan, Y. Li, D. Wu, H. Ma, K. Mao, D. Fan, B. Du, H. Li, and Q. Wei, *Anal. Chim. Acta*, 711 (2012) 24.
30. L. A. Goulart, R. Gonçalves, A. A. Correa, E. C. Pereira, and L. H. Mascaro, *Microchim. Acta*, 185 (2018) 12.
31. L. Ling, J. Xu, Y. Deng, Q. Peng, J. Chen, Y. He, and Y. Nie, *Anal. Methods*, 10 (2018) 2722.